Appl Phys B (2009) 95: 307–314
DOI 10.1007/s00340-008-3321-y

Applied Physics B
Lasers and Optics

Comprehensive study of blue and green multi-quantum-well light-emitting diodes grown on conventional and lateral epitaxial overgrowth GaN

C. Bayram · J.L. Pau · R. McClintock · M. Razeghi

Received: 13 October 2008 / Published online: 29 November 2008

Abstract Growths of blue and green multi-quantum wells (MQWs) and light-emitting diodes (LEDs) are realized on lateral epitaxial overgrowth (LEO) GaN, and compared with identical structures grown on conventional GaN. Atomic force microscopy is used to confirm the significant reduction of dislocations in the wing region of our LEO samples before active-region growth. Differences between surface morphologies of blue and green MQWs are analyzed. These MQWs are integrated into LEDs. All devices show a blue shift in the electroluminescence (EL) peak and narrowing in EL spectra with increasing injection current, both characteristics attributed to the band-gap renormalization. Green LEDs show a larger EL peak shift and a broader EL spectrum due to larger piezoelectric field and more indium segregation in the MQWs, respectively. Blue LEDs on LEO GaN show a higher performance than those on conventional GaN; however, no performance difference is observed for green LEDs on LEO GaN versus conventional GaN. The performance of the green LEDs is shown to be primarily limited by the active layer growth quality.

PACS 81.05.Ea · 81.10.Aj · 81.15.Gh · 85.60.Jb

1 Introduction

Solid-state lighting (SSL) holds the promise of a more energy-efficient, longer-lasting, more compact, and lower maintenance substitute for today's incandescent and fluorescent light sources. Since lighting currently represents about 22% of all electricity consumption, the adoption of SSL could significantly reduce greenhouse gas emissions [1]. Light-emitting diodes (LEDs) based on $In_xGa_{1-x}N$ alloys are currently the most promising candidates for realizing efficient SSL. InGaN is a direct wide bandgap semiconductor with an emission which can span the entire visible spectrum via compositional tuning. However, InGaN LED performance is highly wavelength dependent. Indeed, ultra-bright and efficient blue InGaN-based LEDs are readily available [2] but the efficiency of InGaN-based green LEDs is still far from adequate for use in SSL [3–5].

The lack of economical lattice-matched substrates for the growth of III-nitrides necessitates the usage of GaN-mismatched silicon carbide (SiC) or sapphire (Al_2O_3) substrates, which leads to dislocation densities on the order of 10^8 cm^{-2}. The high performance of blue LEDs in spite of these dislocations is attributed to indium segregation in the InGaN layers that produces nanometer-wide indium-rich regions that behave like quantum dots [6, 7]. These quantum dots (QDs) localize the carriers, and prevent them from recombining non-radiatively at the dislocation sites [8, 9]. Difficulty in realizing high-power green LEDs has three major parts: (1) the limited solubility of indium in InGaN [10] imposes a restricted growth window for the green-emitting InGaN active layer, (2) InGaN with high indium content becomes unstable at elevated growth temperatures required for other layers in the device [11] leading to indium migrating out of the active layers, which reduces the LED spectral quality [4, 11], and (3) InGaN with high indium content generates dislocations leading to lower performance [12].

Blue and green LEDs grown on conventional GaN have been compared in order to study the wavelength-dependent

C. Bayram · J.L. Pau · R. McClintock · M. Razeghi (✉)
Center for Quantum Devices, Department of Electrical Engineering and Computer Science, Northwestern University, Evanston, IL 60208, USA
e-mail: razeghi@eecs.northwestern.edu
Fax: +1-847-4671817

device performance [13–15]. Blue LEDs and laser diodes (LDs) grown on lateral epitaxial overgrowth (LEO) GaN have also been studied in other works, showing superior performance to those grown on conventional GaN [16, 17]. Devices on LEO GaN offer lower leakage current [16, 18, 19], higher stability, better thermal properties [17], and longer device lifetime [20]. Despite these advantages, there are no studies of green active layers and LEDs on LEO GaN. In this work, we analyze blue and green active layers on conventional and high-quality LEO GaN by X-ray diffraction (XRD), atomic force microscopy (AFM), and photoluminescence (PL). Then, we integrate them into LEDs and compare and correlate the material characteristics and device performance.

2 Growth and material characterization

Multi-quantum wells (MQWs) and LEDs were grown on double side polished *c*-plane sapphire substrates in an Aixtron 200/4-HT, horizontal flow, low pressure, metal organic chemical vapor deposition (MOCVD) reactor. Trimethylaluminum (TMAl), trimethylgallium (TMGa), and trimethylindium (TMIn) were the metalorganic cation precursors for Al, Ga, and In, respectively. Bis(cyclopentadienyl)magnesium (Cp_2Mg) and silane (SiH_4) were used as the p- and n-type doping sources, respectively. Ammonia (NH_3) was used as the nitrogen anion source. Nitrogen was used as the carrier gas for growth of the MQWs to help increase indium incorporation, whereas hydrogen was used during the rest of the layers.

2.1 Preparation of high-quality LEO GaN

Growth began with desorption of the sapphire substrate at 1100°C under H_2. Then, a thin low-temperature GaN buffer layer was grown, followed by 2 µm of GaN, grown at 1050°C. In order to create a mask for lateral overgrowth, the wafer was removed from the reactor and 50 nm of silicon nitride (SiN) was deposited by plasma enhanced chemical vapor phase deposition (PECVD) [21] and patterned along the GaN $\langle 1\bar{1}00\rangle$ direction with openings of 2 µm and a period of 15 µm. This pattern direction exposes the A planes $(11\bar{2}0)$ for lateral growth and is known to give the fastest lateral growth rate and high-quality wing regions [22]. For higher device performance, smaller fill factors (ratio of mask opening width to stripe period) are desired, which makes regrowth more challenging [23]. We have used a fill factor of 0.13 to have a larger wing area and to perform better analysis.

Etching of the opening in the SiN layer was performed by electron cyclotron resonance reactive ion etching (ECR-RIE) using an SF_6-based chemistry. We have observed that this ECR-RIE chemistry does not etch GaN appreciably; however, some surface damage is observed by a scanning electron microscope (SEM). Some SiN residuals were observed on the GaN opening regions via AFM. However, when GaN regrowth tests were conducted in these opening regions, a smooth GaN surface was observed via SEM, showing that slight remaining SiN residues did not have a detrimental effect on the GaN regrowth. Proper trade-off must be made between etching time and surface damage, and amount of SiN residual atoms in the GaN opening in correlation with the regrowth characteristics.

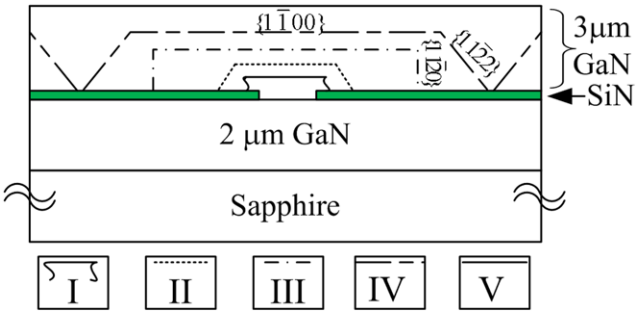

Fig. 1 Schematic sketch of our optimized five-step LEO GaN growth process

After etching, samples were cleaned with trichloroethylene, acetone, and methanol and rinsed thoroughly. Then, samples were placed inside the reactor for our optimized five-step LEO GaN regrowth. A cross-sectional sketch of the LEO GaN steps is shown in Fig. 1.

Step I is designed for high surface diffusion to minimize nucleation on the SiN mask and promote vertical growth on the GaN in the SiN openings in order to create an initial well-formed seed from which the vertical growth will progress. The vertical thickness should be around double the SiN layer thickness. Important growth parameters such as growth temperature, V/III ratio, effective lateral to vertical growth rate ratio, and growth time are given in Table 1.

Step II is similar to step I except that the growth conditions are adjusted to favor both lateral and vertical growth in order to obtain straight side walls [24]. Growth temperature is increased and V/III ratio is decreased, as given in Table 1. If Ga and N adatoms are too mobile, then they tend to align themselves exactly as the etching pattern. However, since the edges of the SiN mask are not perfectly straight lines, this step is needed to achieve better straight side walls. At the end of this step, well-formed inclined $\{11\bar{2}2\}$ facets are observed.

Step III is the lateral growth phase, during which the lateral to vertical (L/V) growth rate is enhanced by increasing the growth temperature [23]. Increasing the effective lateral to vertical growth rate ratio (L/V) decreases the growth time required for coalescence, and helps to bend the threading dislocations sideways [22]. During the first part

Table 1 Important growth parameters for LEO GaN (2-µm opening, 15-µm period): LEO step number, growth temperature (T_{growth} (°C)), V/III ratio, effective lateral to vertical growth rate ratio (L/V), and growth time (t_{growth})

LEO step no.	T_{growth} (°C)	V/III ratio	L/V ratio	t_{growth} (min)
I	1080	6000	1.1	4
II	1100	2930	2.4	60
III	1130	2930	2.6	60
IV	1100	2930	1.4	195
V	1040	2400	1.0	30

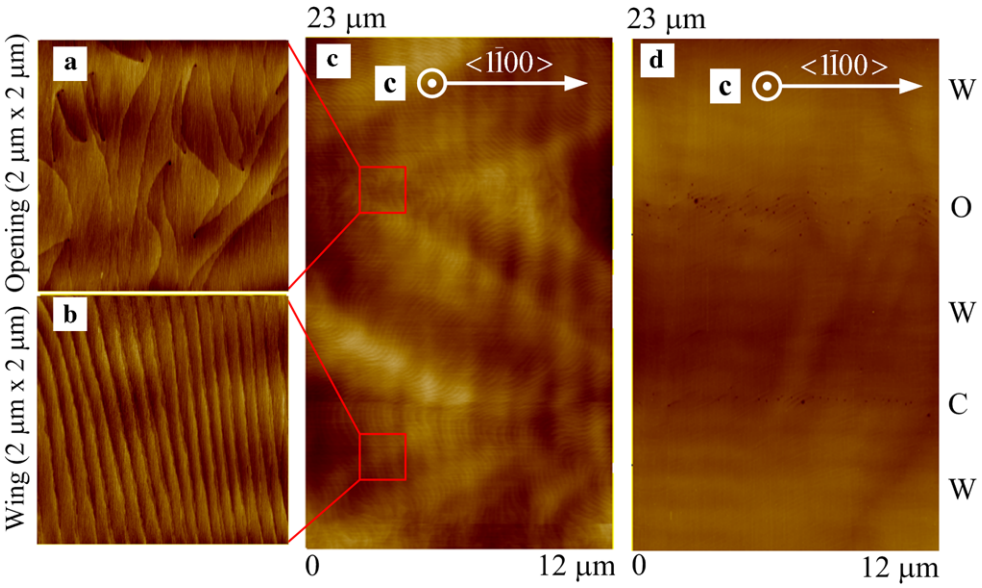

Fig. 2 AFM images of coalesced LEO GaN. **a** Opening (2 µm × 2 µm) and **b** wing (2 µm × 2 µm) have root mean square (RMS) roughness of 1.9 Å and 1.5 Å, respectively. **c** Larger area (12 µm × 23 µm) AFM scan. **d** Dislocations, revealed by hot phosphoric acid treatment, which are seen as *dark spots*. 'W', 'O', and 'C' correspond to wing, opening, and coalescence regions, respectively

of step III the initially inclined $\{11\bar{2}2\}$ side walls begin to tilt, and are replaced with vertical $\{11\bar{2}0\}$ side walls (Fig. 1). This change in the growth direction over the first three steps, from vertical to lateral, helps to bend the threading dislocations sideways so that they do not propagate to the surface.

Step IV is the coalescence step; after the distance between the side walls is close enough, the side-wall slope is increased, as shown in Fig. 1, in order to realize a void-free coalescence front. This is achieved by decreasing the growth temperature sufficiently so that growth favors the formation of inclined $\{11\bar{2}2\}$ facets [23]. This inclination minimizes the voids and prevents the dislocations spreading at the coalescence front. Failure to control the lateral to vertical growth rate during coalescence results in the formation of voids and leads the LEO GaN surface to bend; both can be observed by SEM. During this phase, the lower temperature necessary to realize inclined planes results in less surface diffusion, and the lack of exposed SiN removes the supply of excess adatoms at the facet edge [25]. This results in a slow lateral growth rate, requiring a longer time for full coalescence.

Step V is similar to conventional GaN growth and promotes vertical growth. n-type doping is achieved by introducing SiH_4 during this step, as LEDs will be grown on this template. Typically up to 0.6 µm is grown in this layer. The GaN vertical growth height at full coalescence is ∼5 µm, small enough that wafer bending effects are minimal [26].

Table 1 summarizes the basic growth parameters for the above-explained five-step LEO growth process (Fig. 1) for an opening of 2 µm and a period of 15 µm. It should be possible to reach high-quality LEO GaN for different filling factors and periods, by employing the ideas described in each growth step.

Figure 2 displays the AFM of the fully coalesced LEO GaN templates. The surface above the opening region (Fig. 2a) is similar to that of conventional GaN, exhibiting chaotic atomic steps, the surface termination of which identify screw/mixed type threading dislocations [25]. Contrarily, the wing region (Fig. 2b), where lateral growth occurs, possesses well-ordered parallel atomic steps with no atomic step terminations. The entire surface, including the coalescence region, where the neighboring atomic steps interfere, is observed in Fig. 2c. In order to study the dislocations, a hot (170°C) phosphoric acid (85% H_3PO_4) treatment [19, 27] for 15 min was used. This etch-pit-density study reveals no discernable dislocations in the wing areas, whereas in the LEO GaN coalescence area and opening region dislocation densities of $(2 \pm 1) \times 10^8$ cm^{-2} and $(9 \pm 2) \times 10^8$ cm^{-2} are observed, respectively (Fig. 2d). For comparison, conventional GaN was observed to have

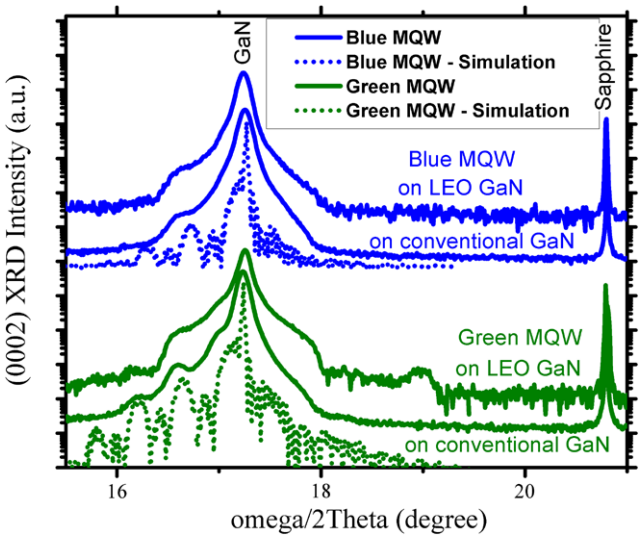

Fig. 3 (0002) XRD omega/2Theta scan of blue and green MQWs on conventional and LEO GaN. The XRD simulation is realized to compare with experimental results

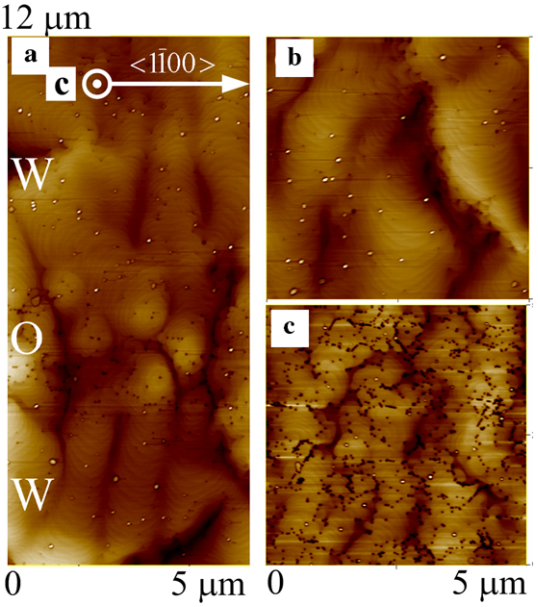

Fig. 4 AFM images of blue MQWs on **a** LEO GaN (5 μm × 12 μm), **b** wing area of LEO GaN (5 μm × 5 μm), **c** conventional GaN (5 μm × 5 μm). 'W' and 'O' correspond to the wing and opening regions, respectively

a dislocation density of $(9 \pm 1) \times 10^8$ cm^{-2}. This phosphoric acid treatment is capable of distinguishing between edge and screw or mixed type dislocations [19, 27]. The bigger pits correspond to dislocations with a screw component whereas smaller ones correspond to edge-type dislocations. It is known that edge-type dislocations may exist in the wing region as their bending is very sensitive to growth conditions [28]. The non-existence of any discernable dislocations in our wing regions shows the quality of the five-step LEO GaN developed, and establishes a baseline from which we can study the effect of dislocations on blue and green InGaN-based LEDs. For LEO GaN, no GaN peak separation is observed (Fig. 3), which shows that there is no significant plane tilt [29], supporting our high-quality growth scheme described.

After preparation of LEO templates as described above, blue and green MQWs and LEDs are grown simultaneously on these templates, and on conventional GaN for comparison purposes. Each quantum well was composed of 3.5-nm-thick InGaN with a 7.0-nm-thick GaN barrier. The thicknesses of the blue and green MQW layers are arranged to be the same in order to have a better comparison. Growth temperatures of the MQWs are adjusted to ensure blue and green luminescence from the InGaN QWs. These MQWs were capped with 550-nm-thick p-GaN to complete the LED structure.

2.2 Blue and green active layers on conventional and LEO GaN

Open-detector X-ray diffraction (XRD) studies and XRD simulations are carried out to confirm the indium composition, and InGaN and GaN thicknesses of the active layer. Figure 3 displays the (0002) XRD (omega/2Theta) scan for three blue and green MQWs on LEO and conventional GaN. The XRD simulations of these MQWs are also plotted, and show good agreement with the experimental data. The InGaN and GaN thicknesses are determined as 3.5 and 7.0 nm, respectively. The indium content in the InGaN well is calculated to be 20% for blue MQWs and 28% for green MQWs. The 0th-order MQW peak is more distinctly observed in green MQWs due to higher average indium content in these structures.

Atomic force microscopy is used to study the surface morphology of the MQW active layers. Figure 4 shows the AFM images of the last barrier of blue MQWs on LEO and conventional GaN. Screw-type threading dislocations are observed to be dominant on the opening (Fig. 4a). Figures 4b and 4c show that the active layer on the wing area has much fewer dislocations and a much smoother surface than that in conventional GaN. This is directly related to the lower dislocation density in the wing area. Figure 5 shows the AFM images of green MQWs on LEO and conventional GaN. Screw-type dislocations are still dominant in the opening region. Although fewer dislocations are observed in the wing than that in the conventional GaN (Figs. 5b and 5c), an island-like (2D) growth is observed to be dominant across the LEO stripe, different from the blue active layer case (Fig. 4). The lower deposition temperature necessary to realize a green active layer results in an island-like growth rather than a layer-by-layer growth as was observed for the blue layer. In summary, the wing regions are observed to be smoother than opening regions.

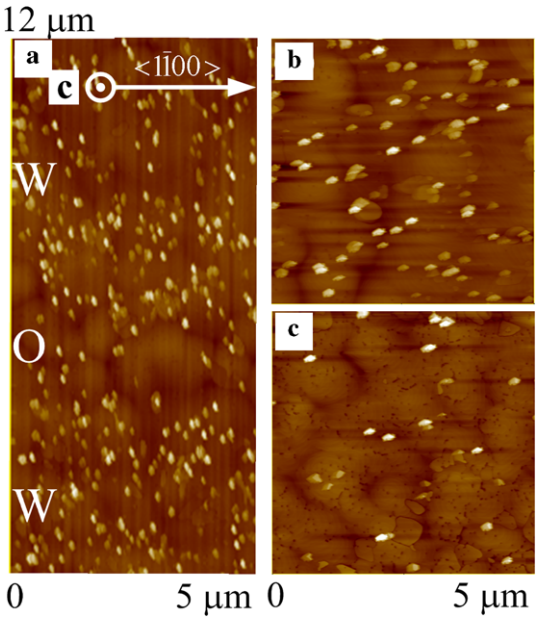

Fig. 5 AFM images of green MQWs on **a** LEO GaN (5 μm × 12 μm), **b** wing area of LEO GaN (5 μm × 5 μm), **c** conventional GaN (5 μm × 5 μm). 'W' and 'O' correspond to the wing and opening regions, respectively

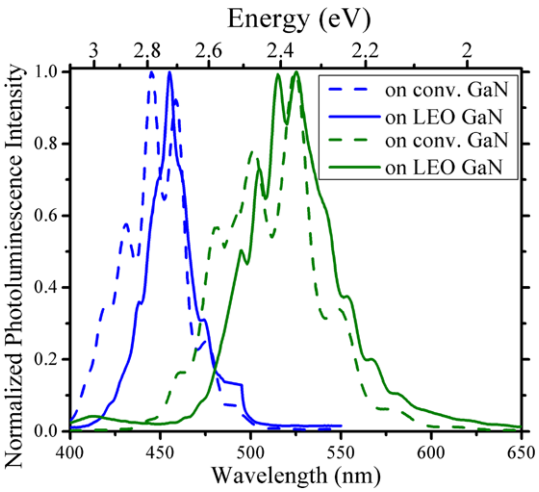

Fig. 6 Room-temperature PL of blue and green active layers

Room-temperature (RT) photoluminescence of these blue- and green-emitting MQWs is shown in Fig. 6. The PL wavelength of MQWs on LEO GaN is observed to be slightly longer than that of the same structure grown on conventional GaN. This could be due to increase in the *c*-plane lattice constant of LEO GaN [30], leading to a smaller compositional pulling effect [31], thus allowing slightly more indium into the InGaN.

2.3 Fabrication of blue and green LEDs on conventional and LEO GaN

Blue and green active layers composed of seven MQWs were grown as described above with the addition of a 550-nm-thick p-GaN capping layer to complete the LED structure. Activation of the p-type GaN is achieved by rapid thermal annealing (RTA) at 1000°C for 30 s in nitrogen ambient. After this, the surface is treated with HCl:H_2O (1:1) and 30 Å Ni/30 Å Au is deposited and annealed for 10 min under air to achieve a transparent ohmic contact to p-GaN. ECR-RIE ($SiCl_4$:Ar-based chemistry) is used to etch 300 μm × 300 μm mesas; thus, each LED mesa spans many opening, wing, and coalescence regions. Finally, 400 Å Ti/1200 Å Au is deposited as a thick n-type contact and to serve as a central bond pad on top of the thin transparent p-contact in order to complete the LED fabrication.

3 Device results and discussion

The blue and green LEDs on conventional GaN are hereinafter referred to as '$B_{Conv.}$' and '$G_{Conv.}$', whereas those on LEO GaN are referred to as 'B_{LEO}' and 'G_{LEO}', respectively. Figures 7a and 7b show the I–V curves of blue and green LEDs on conventional and LEO GaN. A clear improvement in reverse-bias leakage characteristics is observed between samples B_{LEO} and $B_{Conv.}$, whereas no significant difference is observed between samples $G_{Conv.}$ and G_{LEO}.

Reverse-bias characteristics of the LEDs are studied in detail. The majority of the leakage current is expected to flow through the LED, with only a small portion contributed by surface leakage [32]. The leakage current through nitride p–i–n devices is known to be dominated by hopping of charge carriers via localized defect-related states (traps) in the depletion region [33, 34]. In the case of defect-dominated reverse conduction, the reverse I–V characteristics of LEDs can be modeled as [19]

$$I = I_0 e^{qV/E_0}, \tag{1}$$

where V and E_0 are the diode voltage and the energy parameter, respectively, with I_0 being a pre-exponential factor. E_0 represents the electrical activities of dislocations with a screw component, and is known to be dependent on the voltage at which the fitting is realized [19, 33, 34]. For electrical fields $E \ll (2kT/qa) \approx 5 \times 10^5$ V/cm (assuming that a, the localization radius of the electron wave function, is 10 Å), thermionic emission over a barrier dominates the leakage current [18]. We have used the fitting in the low-voltage range ($1 < V < 5$). In this range, I_0 and E_0 are related to the density and to the electrical activities of dislocations with a screw component, respectively [19, 32–35]. Using (1) to fit

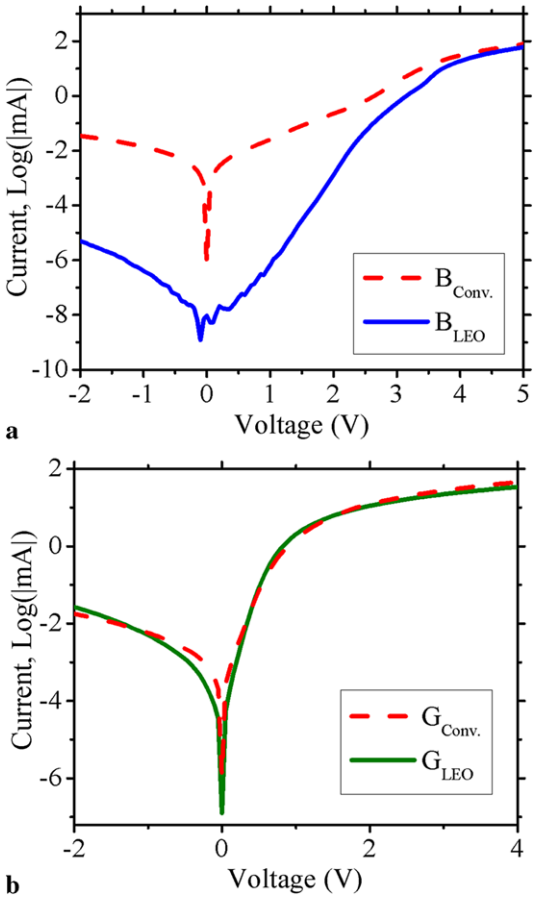

Fig. 7 Current–voltage curves (logarithmic scale) of **a** blue and **b** green LEDs on conventional ($B_{Conv.}$, $G_{Conv.}$) and LEO GaN (B_{LEO}, G_{LEO})

Table 2 Important calculated/fitted LED parameters: leakage-current pre-exponential factor (I_0) and electrical activities of dislocations with a screw component factor (E_0)

Identifier	Device	I_0 (μA)	E_0 (eV)
$B_{Conv.}$	Blue LED on conventional GaN	7.86×10^{-6}	1.34
B_{LEO}	Blue LED on LEO GaN	3.17×10^{-10}	0.73
$G_{Conv.}$	Green LED on conventional GaN	2.01×10^{-6}	0.91
G_{LEO}	Green LED on LEO GaN	2.16×10^{-6}	0.80

the I–V curves, reverse-bias parameters I_0 and E_0 are calculated and given in Table 2.

I_0 is related to the square of the density of dislocations with a screw component [19]. Comparing I_0 values among the different samples in Table 2 suggests that B_{LEO} has approximately two orders of magnitude lower dislocation density than $B_{Conv.}$. This agrees with the etch-pit-density study of the LEO GaN (Fig. 2). For $G_{Conv.}$ and G_{LEO}, no significant difference in I_0 is observed. As the same LEO GaN templates are used for B_{LEO} and G_{LEO}, the active layer used in samples $G_{Conv.}$ and G_{LEO} is the dominant dislocation generator leading to a uniform dislocation distribution through the active layer. This helps explaining why we do not see a significant difference in I_0 between samples $B_{Conv.}$, $G_{Conv.}$, and G_{LEO}.

E_0 is very sensitive to the growth conditions [19]; thus, blue ($B_{Conv.}$ and B_{LEO}) and green ($G_{Conv.}$ and G_{LEO}) emitters should be considered separately. The lower value for sample B_{LEO} compared to $B_{Conv.}$ could be due to periodic alignment of the dislocations leading to a stronger voltage dependency of leakage current. A similar trend is observed between G_{LEO} and $G_{Conv.}$; however, it is less pronounced, due to the generation of additional dislocations in the active layer creating an almost homogeneous dislocation density similar to conventional GaN (Figs. 4 and 5). The higher active layer quality of sample $B_{Conv.}$ compared to $G_{Conv.}$ could be the reason for the higher value of E_0 leading to smaller dependency of leakage current on voltage.

Electroluminescence (EL) spectra were acquired for the LEDs under pulsed current injection (duty cycle of 10% and frequency of 5 kHz) in order to help reduce heating effects under higher current injection (Figs. 8 and 9). The minimal role of heating was confirmed by measuring the peak intensity versus power and noting that, for the currents used in this study, no thermal roll-over was observed to occur. The EL spectra of blue LEDs are shown in Fig. 8. The inset shows that both devices demonstrate a blue shift (from 465 to 446 nm) with increasing current. The decrease of wavelength with injection current is attributed to band-gap renormalization (due to free-carrier screening of the piezoelectric (PE) field). At all but the lowest currents, B_{LEO} has a slightly longer wavelength emission than $B_{Conv.}$ (Fig. 8, inset). In previous blue LED studies, a similar observation has been reported [16]. This observation is in agreement with the PL that was discussed in Sect. 2.2. Device B_{LEO} has a narrower EL spectra than $B_{Conv.}$ (Fig. 10). This suggests a more uniform indium distribution throughout the active layer [7]. Indeed, Fig. 4 directly illustrates the more uniform surface of blue MQWs on LEO GaN, supporting the advantage of LEO templates.

In Fig. 10 the EL FWHMs of the blue LEDs are plotted as a function of the injection current; the FWHM of the device on conventional GaN can be seen to decrease with current, while the FWHM of the device on LEO GaN can be seen to increase. The EL FWHM broadening in B_{LEO} could be related to dislocation alignment in the LEO openings resulting in an electrical field build up.

The EL spectra of the green LEDs are shown in Fig. 9. Device G_{LEO} is observed to have longer peak wavelength than device $G_{Conv.}$ (Fig. 9, inset). With increasing current, the EL FWHM increased for both devices (Fig. 10); however, the EL peak shift of sample G_{LEO} is larger than that

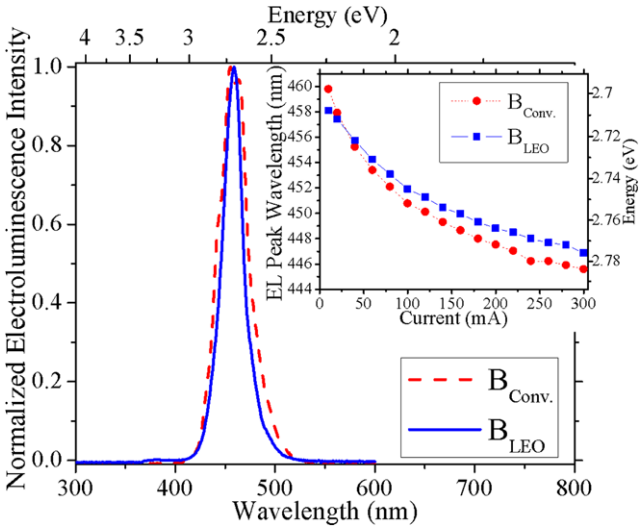

Fig. 8 Electroluminescence spectra of blue LED on conventional ($B_{Conv.}$) and LEO GaN (B_{LEO}) under 20-mA current injection. *Inset* displays the peak wavelength at different current injections

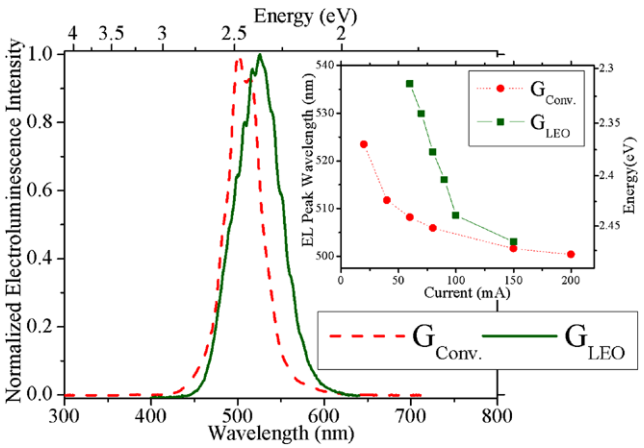

Fig. 9 Electroluminescence spectra of green LED on conventional ($G_{Conv.}$) and LEO GaN (G_{LEO}) under 80-mA current injection. *Inset* displays the peak wavelength at different current injections

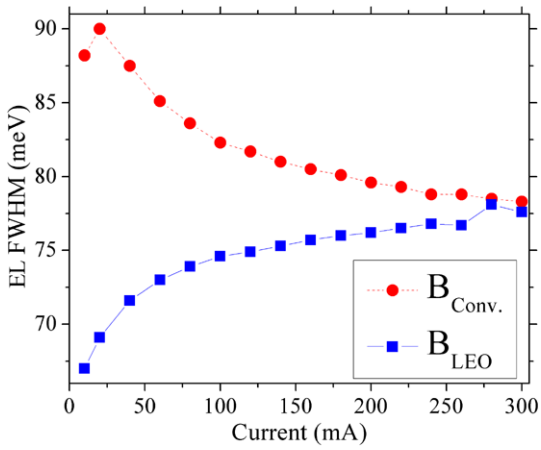

Fig. 10 EL FWHM dependency on current for blue LED on conventional ($B_{Conv.}$) and LEO GaN (B_{LEO})

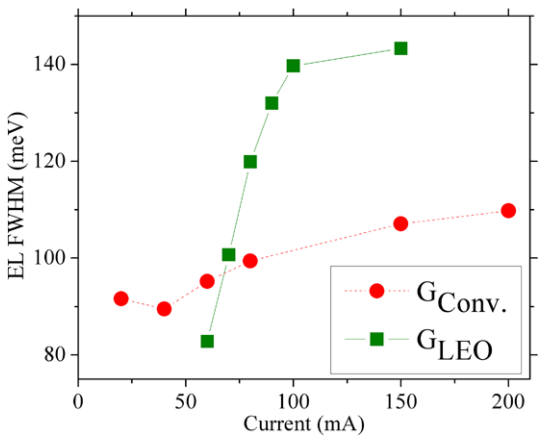

Fig. 11 EL FWHM dependency on current for green LED on conventional ($G_{Conv.}$) and LEO GaN (G_{LEO})

of G_{LEO}, possibly due to the effects of piezoelectric fields. These piezoelectric fields may also be responsible for the broader EL FWHM observed in green LEDs. (This could be seen by comparing the ordinates of Figs. 10 and 11.)

Comparing blue and green LEDs, a more pronounced EL peak shift is observed for green LEDs. This suggests stronger piezoelectric effects in the active layer. Piezoelectric effects are expected to be more pronounced in green MQWs due to the higher indium content of the layers [14]. The broader EL FWHMs of green LEDs than those of blue ones indicates a bigger indium fluctuation through the green active layer [7]. This is in agreement with the AFM measurements we have discussed in Sect. 2.1 (Figs. 4 and 5).

The radiant power of the various devices was measured as a function of injection current in continuous-wave injection (not shown). Device B_{LEO} achieved 2.6 times more power than $B_{Conv.}$, whereas G_{LEO} and $G_{Conv.}$ had almost the same peak power independent of the template. In near-field EL studies of device B_{LEO}, we have observed a stronger luminescence originating from the wing regions compared to the opening regions. This luminescence difference should be related to the density of dislocations in the corresponding regions, demonstrating the role of dislocations as non-radiative recombination centers [9]. For $G_{Conv.}$ and G_{LEO}, we did not observe any difference between luminescence in the wing and opening regions. This supports our reverse-bias analysis, and reinforces that the green LED performance is dominated primarily by the active-ayer quality. In summary, green MQW quality should be improved to reveal the benefits of GaN LEO templates in green LEDs.

4 Summary and conclusion

A five-step LEO GaN growth technique for high-quality LEO GaN growth is introduced. Blue- and green-emitting active layers and LEDs on conventional GaN and five-step-grown LEO GaN templates are realized. AFM, XRD, and PL are used to study the structural and optical properties of the active layers, and the effects of dislocations on blue and green active layers are identified. Significant differences in blue and green active layer surfaces are analyzed. The high-quality LEO templates are observed to be important for smoother active layer surface morphologies. Blue and green LEDs on conventional GaN and high-quality LEO GaN are studied. Green LEDs are observed to be leakier than blue ones, and no significant differences between green LEDs on conventional GaN and LEO GaN in terms of I–V behavior and peak power are observed. Green MQW quality is determined to be the bottleneck for high-performance green emitters, not template dislocation density.

Acknowledgements The authors would like to thank Dr. P. Kung for valuable discussions regarding LEO growth, and also acknowledge the Fulbright Association and the Spanish Ministry of Education and Science for supporting one of the authors (J.L.P.).

References

1. C.J. Humphreys, MRS Bull. **33**, 459 (2008)
2. N.F. Gardner, G.O. Muller, Y.C. Shen, G. Chen, S. Watanabe, W. Gotz, M.R. Krames, Appl. Phys. Lett. **91**, 243506 (2007)
3. Y.H. Cho, S.K. Lee, H.S. Kwack, J.Y. Kim, K.S. Lim, H.M. Kim, T.W. Kang, S.N. Lee, M.S. Seon, O.H. Nam, Y.J. Park, Appl. Phys. Lett. **83**, 2578 (2003)
4. I.K. Park, M.K. Kwon, J.O. Kim, S.B. Seo, J.Y. Kim, J.H. Lim, S.J. Park, Y.S. Kim, Appl. Phys. Lett. **91**, 133105 (2007)
5. C. Bayram, F.H. Teherani, D. Rogers, M. Razeghi, Appl. Phys. Lett. **93**, 081111 (2008)
6. Y. Narukawa, Y. Kawakami, M. Funato, S. Fujita, S. Nakamura, Appl. Phys. Lett. **70**, 981 (1996)
7. M. Takeguchi, M.R. McCartney, D.J. Smith, Appl. Phys. Lett. **84**, 2103 (2004)
8. S.J. Rosner, E.C. Carr, M.J. Ludowise, G. Girolami, H.I. Erikson, Appl. Phys. Lett. **70**, 420 (1996)
9. S.F. Chichibu, H. Marchand, M.S. Minsky, S. Keller, P.T. Fini, J.P. Ibbetson, S.B. Fleischer, J.S. Speck, J.E. Bowers, E. Hu, U.K. Mishra, S.P. DenBaars, T. Deguchi, T. Sota, S. Nakamura, Appl. Phys. Lett. **74**, 1460 (1999)
10. I. Ho, G.B. Stringfellow, Appl. Phys. Lett. **69**, 2701 (1996)
11. B. Van Daele, G. Van Tendeloo, K. Jacobs, I. Moerman, M.R. Leys, Appl. Phys. Lett. **85**, 4379 (2004)
12. C. Wetzel, T. Salagaj, T. Detchprohm, P. Li, J.S. Nelson, Appl. Phys. Lett. **85**, 866 (2004)
13. S. Nakamura, M. Senoh, N. Iwasa, S. Nagahama, Jpn. J. Appl. Phys. **34**, L797 (1995)
14. S.J. Chang, W.C. Lai, Y.K. Su, J.F. Chen, C.H. Liu, U.H. Liaw, IEEE J. Sel. Top. Quantum Electron. **8**, 278 (2002)
15. Y.D. Qi, H. Liang, D. Wang, Z.D. Lu, W. Tang, K.M. Lau, Appl. Phys. Lett. **86**, 101903 (2005)
16. T. Mukai, K. Takekawa, S. Nakamura, Jpn. J. Appl. Phys. **27**, L839 (1998)
17. D.I. Florescu, V.M. Asnin, F.H. Pollak, A.M. Jones, J.C. Ramer, M.J. Schurman, I. Ferguson, Appl. Phys. Lett. **77**, 1464 (2000)
18. P. Kozodoy, J.P. Ibbetson, M. Marchand, P.T. Fini, S. Keller, J.S. Speck, S.P. Denbaars, U.K. Mishra, Appl. Phys. Lett. **73**, 975 (1998)
19. D.S. Li, H. Chen, H.B. Yu, H.Q. Jia, Q. Huang, J.M. Zhou, J. Appl. Phys. **96**, 1111 (2004)
20. S. Tomiya, T. Hino, S. Goto, M. Takeya, M. Ikeda, IEEE J. Sel. Top. Quantum Electron. **10**, 1277 (2004)
21. S. Tomiya, K. Funato, T. Asatsuma, T. Hino, S. Kijima, T. Asano, M. Ikeda, Appl. Phys. Lett. **77**, 636 (2000)
22. A.E. Romanov, P. Fini, J.S. Speck, J. Appl. Phys. **93**, 106 (2003)
23. H. Marchand, J.P. Ibbetson, P.T. Fini, S. Keller, S.P. DenBaars, J.S. Speck, U.K. Mishra, J. Cryst. Growth **195**, 328 (1998)
24. D. Kapolnek, S. Keller, R. Vetury, R.D. Underwood, P. Kozodoy, S.P. Denbaars, U.K. Mishra, Appl. Phys. Lett. **71**, 1204 (1997)
25. H. Marchand, X.H. Wu, J.P. Ibbetson, P.T. Fini, P. Kozodoy, S. Keller, J.S. Speck, S.P. Denbaars, U.K. Mishra, Appl. Phys. Lett. **73**, 747 (1998)
26. M. Takeya, K. Yanashima, T. Asano, T. Hino, S. Ikeda, K. Shibuya, S. Kijima, T. Tojuo, S. Ansai, S. Uchida, Y. Yabuki, T. Aoki, T. Asatsuma, M. Ozawa, T. Kobayashi, E. Morita, M. Ikeda, J. Cryst. Growth **221**, 646 (2000)
27. X. Xu, R.P. Vaudo, J. Flynn, G.R. Brandes, J. Electron. Mater. **31**, 402 (2002)
28. A. Sakai, H. Sunakawa, A. Usui, Appl. Phys. Lett. **73**, 481 (1998)
29. P. Fini, H. Marchand, J.P. Ibbetson, S.P. Denbaars, U.K. Mishra, J.S. Speck, J. Cryst. Growth **209**, 581 (2000)
30. J.Z. Domagala, Z.R. Zytkiewicz, B. Beaumont, J. Kozlowski, R. Czernetzki, P. Prystawko, M. Leszczynski, J. Cryst. Growth **245**, 37 (2002)
31. K. Hiramatsu, Y. Kawaguchi, M. Shimizu, N. Sawaki, T. Zheleva, R.F. Davis, H. Tsuda, W. Taki, N. Kuwano, K. Oki, MRS Internet J. Nitride Semicond. Res. **2**, 6 (1997)
32. M.S. Ferdous, X. Wang, M.N. Fairchild, S.D. Hersee, Appl. Phys. Lett. **91**, 231107 (2007)
33. D.V. Kuksenkov, H. Temkin, A. Osinsky, R. Gaska, M.A. Khan, J. Appl. Phys. **83**, 2142 (1998)
34. D.V. Kuksenkov, H. Temkin, A. Osinsky, R. Gaska, M.A. Khan, Appl. Phys. Lett. **72**, 1365 (1998)
35. J.W.P. Hsu, M.J. Manfra, D.V. Lang, S. Richter, S.N.G. Chu, A.M. Sergent, R.N. Kleiman, L.N. Pfeiffer, R.J. Molnar, Appl. Phys. Lett. **78**, 1685 (2001)